06

High-temperature transformation of polymineral complex structures

© A.G. Chetverikova,[1] V.N. Makarov,[1] O.N. Kanygina,[1] M.M. Seregin,[2] V.L. Berdinskiy,[1] A.B. Kanaki,[3] E.S. Deeva,[3] A.A. Smorokov,[4] M.S. Syrtanov,[4] E.B. Gello[5]

[1]Orenburg State University,
460018 Orenburg, Russia
[2]LLC BO-ENERGO.ASTS,
129090 Moscow, Russia
[3]JSC TomskNIPIneft,
634027 Tomsk, Russia
[4]Tomsk Polytechnic University,
634028 Tomsk, Russia
[5]LLC Ackermann Cement,
462360 Novotroitsk, Orenburg region, Russia
e-mail: KR-727@mail.ru

Received June 30, 2023
Revised November 8, 2023
Accepted November 13, 2023

The combination of various microcrystalline structures of natural polymineral complexes determines the main trends in their practical application. For example, the extraction of rare and trace chemical elements isomorphically incorporated into crystalline cells involves mechanical and thermal means of modifying and destroying durable aluminosilicate structures. The qualitative and quantitative composition of impurity elements, phase transformations and fine structure were established using diffractometry, differential thermal and spectral analyses. The presence of paramagnetic impurity ions Fe^{3+}, Cu^{2+} and Mn^{2+} allows them to be used as spin probes for recording the processes of modification and destruction of crystal cells using ESR spectroscopy.

Keywords: crystal cell, X-ray phase analysis, impurity ions, spectroscopy.

DOI: 10.61011/JTF.2024.01.56907.167-23

Introduction

The natural „synthesis“ of materials, which took place, as a rule, at high pressures and temperatures for a long time, results in the formation of many crystalline minerals. The synthesis of similar substances is either very difficult or impossible at all in laboratory conditions. They retain their original crystal structure, at least at the micro level. even in the processes of long-term mechanical transformations and grinding

During their formation, their regular crystal lattices were filled with various impurity elements, many of which are valuable hard-to-recover raw materials. Extraction of such rare and scattered elements is a complex technological process, for example, from aluminosilicate gratings. As a rule, it includes grinding and high-temperature processing. The purpose of such operations is the destruction of crystal structures for the subsequent physico-chemical extraction of atoms and ions of impurity elements.

Both the parameters of crystal lattices and the curves of temperature evolutions up to destruction are known for artificial and pure crystals. The evidence becomes less obvious for structures synthesized by nature. The technological process always has several stages at which the evolution of the material structure from a given trajectory may begin to deviate. The impurity centers begin to swing the process of destruction of crystal lattices out of equilibrium in addition to the external fluctuating production conditions. The presence of impurity centers is sometimes not monitored, sometimes ignored, although they can serve both as activators [1] and stabilizers of phase and polymorphic transformations [2]. The impurity centers can be inert in a specific technological process and act simply as indicators of structural transformations [3]. Paramagnetic impurity ions, such as Mn^{2+} and Fe^{3+}, are spin labels allowing for using the ESR method to record the Jahn-Teller effects affecting the energy of crystal cells containing these ions [4].

Dispersed systems, on the one hand, inherit the properties of macro-objects, on the other hand, exhibit the unpredictability of the evolution of natural polymineral complexes (NPC) due to possible synergistic effects. The study of the structural, physico-chemical and technological properties of the NPC of various deposits will expand the raw material base for various industries [5–9].

The purpose of this work is to study the high-temperature transformation of crystal structures and to determine the role of impurity centers in the stabilization, distortion or destruction of crystal lattices of minerals that make up NPC.

Table 1. Chemical composition of NPC particles, wt.%

Oxide	SiO_2	Al_2O_3	CaO	Fe_2O_3	MgO	K_2O	TiO_2	Na_2O	SO_3	Loss on ignition
Table of Content	50.46	12.66	8.71	6.05	3.61	2.13	0.82	0.71	0.21	14.64

1. Experimental

1.1. Material

The NPC of the Yuzhno-Uralskoe deposit in the Orenburg region, developed by LLC „Ackermann Cement" were studied.

The chemical composition analysis conducted in accordance with the Russian standard GOST 21216-2014 [10] showed the presence of basic oxides in the NPC, listed in descending order in Table 1. The average values obtained from 10 representative samples of the deposit are indicated in weight percentages; the measurement accuracy was 0.01 wt.fluctuation of the oxide contents in the sample across various sampling locations was less than 5.5 wt.%.

The studied NPC were classified in accordance with GOST 9169-2021 as acidic non-metallic feedstock ($< 14\%$ Al_2O_3) with a high content of coloring oxides ($> 5\%$ $Fe_2O_3 + TiO_2$) and low content of water-soluble salts. Powders consisting of particles with an effective diameter of less than $40\,\mu$m were used to study the structural transformations of the components of a thermally exposed NPC. The specified dispersion was achieved by dry grinding in a laboratory ball mill (iMold, Russia) and subsequent screening on a sieve with a mesh size of $40\,\mu$m (if more complex sample preparation was not required for more accurate analysis). The isoelectric point of the NPC, determined according to [11], close to $pH \approx 8.3$ [12].

Modeling and understanding the full picture of structural transformations occurring with increasing temperature requires a complex of experimental studies at different hierarchical levels: micro- and nanoscale. The reliability of the information is ensured by the fact that the analyses and their interpretation were carried out in four scientific laboratories with different instrumentation and software. The results with a high degree of correlation have been accepted as reliable data. Methods allowing the evaluation of qualitative and quantitative compositions of impurity elements (section 1.2), mineral characteristics (section 1.3−1.5) and the fine structure were used in this study (methods (sections 1.5, 1.6)).

1.2. X-ray fluorescence analysis (XRF)

The XRF made it possible to clarify the elemental composition of the studied material, since two devices were used for the study, each of which allowed considering an individual range of chemical elements with both large and small atomic masses.

In the first case, the spectra were recorded using an energy dispersive X-ray fluorescence spectrometer ARL Quant'X (Thermo Fisher Scientific, USA). Conditions for recording of spectra: tube anode — rhodium; tube power — 50 W; cooling — air; atmosphere: vacuum for analysis of elements from aluminum to scandium; air for analysis of elements from titanium to uranium. The analysis of powders under vacuum was carried out in a gas-permeable cuvette.

In the second case, the X-ray spectra were recorded using the SPECTROSCAN MAX-GVM analytical complex (LLC „NPO „SPECTRON", Russia) based on a vacuum X-ray fluorescence crystal diffraction scanning spectrometer. The measurements were carried out under normal laboratory conditions at a temperature of $20 \pm 5^\circ$C. Standard samples were used to calculate the coefficients of proportionality and build calibration curves „Calibration Sample GR PA5.700.001", „Calibration Sample MgO PA5.700.001-02" etc. The standard samples 10021-2011, 10017-2011, 10019-2011, 10015-2011, 10018-2011 were used to test the accuracy of the measuring instruments.

1.3. X-ray diffraction analysis

The analysis of powder samples to determine the phase composition was performed using two DRON-type devices. Semi-quantitative mineralogical analysis of the initial sample of NPC was conducted as a detailed analysis of the clay mineral proportion using an X-ray diffractometer RIGAKU ULTIMA IV (Rigaku Corporation, Japan) with the X-ray imaging in the Bregg-Brentano geometry. Diffractograms were obtained under the following conditions: X-ray tube anode — Cu (copper), tube voltage — 40 kV, current — 30 mA, power — 1.2 kW, shooting speed — 1 deg/min, step 0.02°, imaging angles 2θ from 3° to 65°. The interpretation of diffractograms consisted of the stages of identification of the phase composition, crystal modifications and assessment of their quantitative content by full-profile analysis methods (Rietveld method). Diffractograms were processed using special software products (PDXL, Traces V6, SiroQuant) and digital databases of X-ray powder diffractometry PDF2 or PDF4 of the International Centre for Diffraction Data (ICDD, Denver, USA). The error in calculating the quantitative content of each mineral phase did not exceed 10%, and depended on the ratio of peak intensity of the main, significant and secondary phases [13].

The analysis of the evolution of the phase composition as a result of heat treatment did not require specific shooting conditions and interpretation of radiographs. Therefore, Shimadzu XRD 7000S diffractometer (Shimadzu Corporation, Japan) equipped with a OneSight matrix detector was used. Diffractograms were taken at the following parameters: X-ray tube anode — Cu (copper), powder

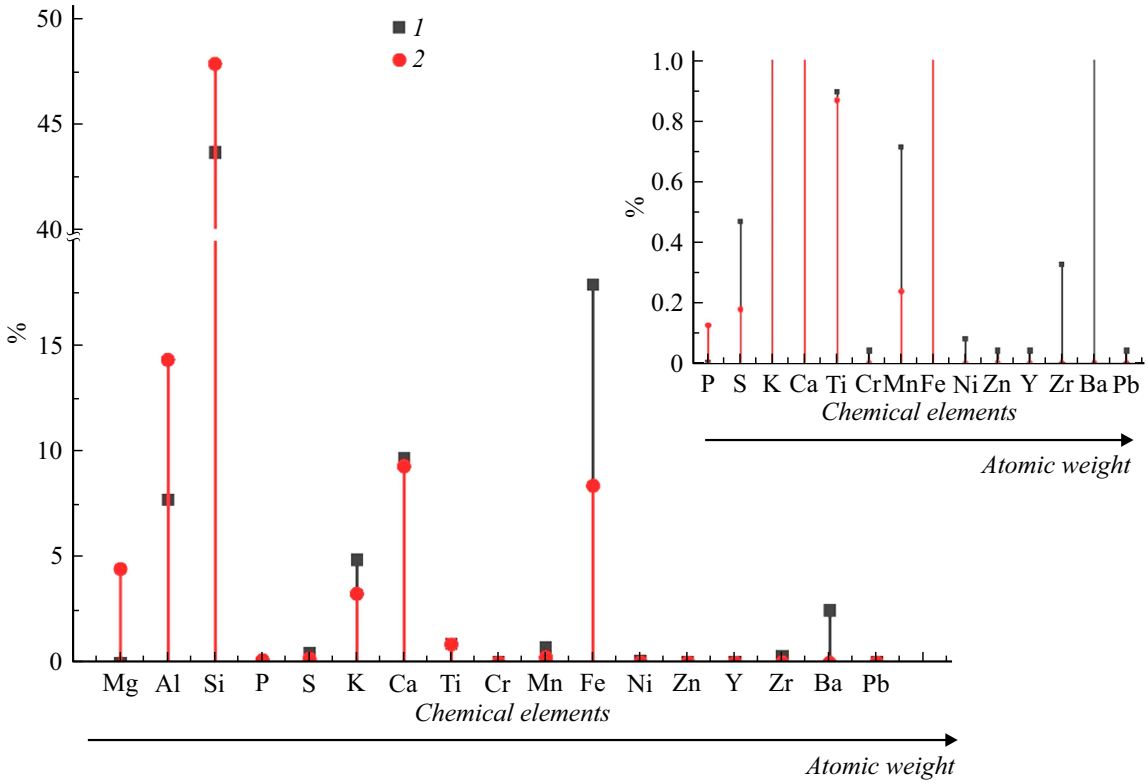

Figure 1. The result of the XRF obtained by two methods: *1* — ARL Quant'X; *2* — SPECTROSCAN MAX-GVM).

sample with rotation, shooting angles 2θ from 5 to 140°, shooting speed — 1°/min, step — 0.2°.

1.4. Differential thermal analysis and thermogravimetric analysis (DTA/TGA)

The structural transformation processes in the sample were first monitored using differential thermal analysis. DTA thermograms were obtained using Thermoscan-2 system (manufacturer country — Russia) with a heating rate of 10°C/min [14] from room temperature 25 to 1000°C, the temperature measurement error was ±1°C. Aluminum oxide powder (Al_2O_3) weighing 0.5 g, sealed in a quartz vessel, was used as a reference. The weight of the test sample placed in a quartz crucible was 0.50 ± 0.01 g. Gravimetric analysis was performed using analyzer SDT Q600 (INTERTECH Corporation, USA). Imaging conditions: ceramic (Al_2O_3) crucibles; atmosphere — air; air consumption — 100 ml/min.

1.5. Infrared (IR) spectroscopy

The spectra of the studied samples were obtained using the Fourier-IR spectrometer InfraLUM FT-08 (Lumex LLC, Russia). Zinc selenide (ZnSe) with a single reflection was used as a crystal for the attenuated total reflectance (ATR) accessory. Measurements were conducted in the range 550–4000 cm^{-1} with a resolution of 2 cm^{-1}, Bessel apodization was used for the Fourier transform.

The spectra were recorded using accumulation mode with 60 scans and baseline correction. A continuous wavelet transform was applied to search for absorption maxima, decomposing the analyzed spectrum using MHAT wavelets with a width from 1 to 25 cm^{-1}. The wavelet analysis made it possible to identify local maxima of overlapping peaks [15].

1.6. ESR spectroscopy

The electron paramagnetic resonance spectra of NPC samples in the initial state and after reference temperatures were recorded using small-sized automated ESR spectrometer CMS8400 (Adani, Belarus) at room temperature. ESR spectrum recording: frequency 9.86 GHz, magnetic field 0.1–0.6 T, frequency of magnetic field modulation — 100 kHz.

2. Results and discussion

2.1. Updated chemical composition of NPC particles

The resulting chemical oxide composition of NPC meets the requirements for the random distribution of the oxide composition of non-metallic raw materials intended for industrial use [16]. The updated elemental composition is illustrated in Fig. 1. NPC particles contain 17 chemical elements, most of which are transition metals. Eight metals

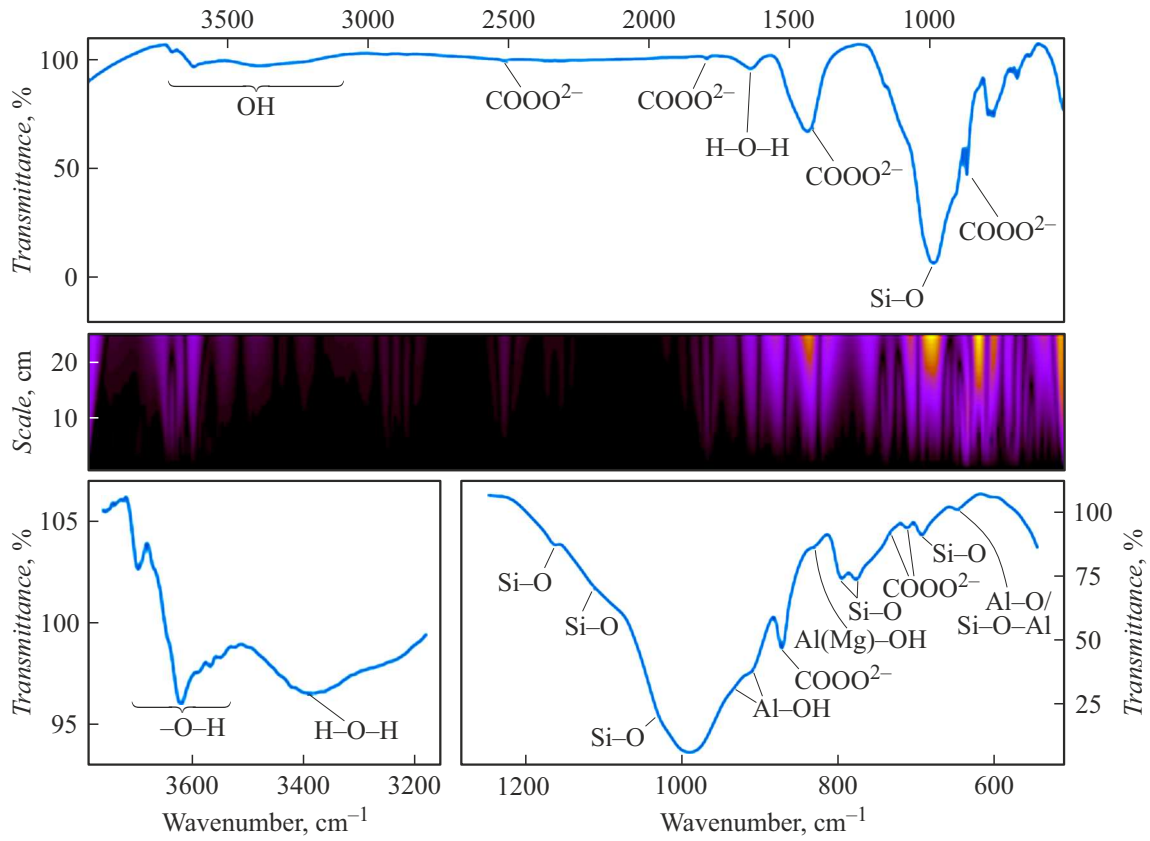

Figure 2. IR spectrum of NPC powders (top); wavelet transform of the spectrum (middle insert); fragments of the most saturated absorption bands of the spectrum (bottom).

with the concentration of less than 1% are classified as impurities (insert in Fig. 1): Ti, Cr, Mn, Ni, Zn, Zr and Pb. Trace amounts of copper, vanadium, and yttrium were found. The presence of such elements such as Fe, Ti, Cr, Mn, and Ni in the sample makes it feasible to use the ESR spectroscopy to study the fine structure. The presence of ions Fe^{3+} and Mn^{2+} in the NPC determined the logic of their use as well-proven paired spin labels [17].

The spread of values for Fe, Al and Si is attributable to the fact that these elements are contained both in the crystal lattices of „native" minerals (for example, iron oxides/hydroxides, silica, alumina) and are present in the form of impurity centers (carbonates, clay minerals).

2.2. Chemical bonds in NPC minerals

Fig. 2 shows the results of IR spectroscopy of the NPC. The main absorption maximum was in the range of $800-1200\,cm^{-1}$, in which, first of all, Si-O and Al-OH bonds determine characteristic absorption bands of the aluminosilicate group of minerals. The librations of the Al-OH bond (933, $908\,cm^{-1}$) and fluctuations of the Si-O bond (991, 1030, 1114 and $1161\,cm^{-1}$) of the kaolinite mineral were the most intensive among them. Many of these broad absorption bands included weaker bands belonging, in particular, to montmorillonite (smectite) or clinochlorite (magnesian chlorite). The qualitative determination of these minerals is impossible by the conventional IR spectroscopy method due to the small quantitative content and weak resolution of absorption bands due to the similarity of structures.

It was possible to separate the overlapping lines (the lower part of Fig. 2) as a result of the wavelet transform (the middle part of Fig. 2) and spread the absorption bands across the corresponding minerals (Table 2).

The mode with a maximum in the region of 828 cm^1 indicated that kaolinite was the main clay mineral in the sample. This mode was caused by the excitation of some „defective" Al-OH groups in which the cation Al^{3+} is replaced by an ion Mg^{2+}. Such isomorphism was confirmed by the absorption band at $685\,cm^{-1}$, related to the deformation oscillation of Al(Mg)-OH. Narrow intense maxima in the region of $3620-3700\,cm^{-1}$ indicated vibrations of Me-OH, where Me is the metal of the crystal lattice, rather than valence vibrations of OH groups. Therefore, the absorptions at frequencies 3621, 3645, 3672, $3696\,cm^{-1}$ were caused by vibrations of various OH groups in the structure of the kaolinite crystal: one group was inside the crystal and three other groups were in the interlayer space of kaolinite.

A broad maximum was observed in the region $1600-1700\,cm^{-1}$. It was formed by the excitation of deformation vibrations of water molecules in the interlayer space

Table 2. Distribution of absorption bands of minerals

Mineral, Chemical formula, Spatial symmetry group, Mineral nomenclature	Band absorption, cm^{-1}	Chemical bond (type of oscillation)
Kaolinite $Al_4[Si_4O_{10}](OH)_8$ P1 Two-layer lattice of silicon-oxygen tetrahedral and alumina-oxygen octahedral layers	649	Al-O (tensioning) Si-O-Al (broadcast) [21–23]
	685	Al(Mg)-OH (deformation) [21,22,24]
	828	Al(Mg)-OH libration [21,22]
	908	Al-OH (libration)
	933	[21–23,25]
	1030	Si-O (antisymmetric stretching) [23]
	3621	O-H (valence, inside the crystal) [21,22,26]
	3645, 3672, 3696	O−H (valence, interlayer) [21,22,25,27]
Quartz SiO_2 $P3_121$ Lattice of silicon-oxygen layer	693 777, 796	Si−O [28]
Calcite $CaCo_3$ $R\bar{3}c$ Anhydrous carbonate	712, 733 873 1415, 1436 1797, 2514	$COOO^{2-}$ [18]
Montmorillonite $\left((Mg_{0.33}Al_{1.67}[Si_4O_{10}](OH)_2[Na_{0.33}(H_2O_4)]\right)$ $B2/m$ Three-layer lattice of two silicon-oxygen tetrahedral and, aluminum oxygen separating them octahedral, layers	908	Al-OH (libration) [21–23,25]
	991	Si-O (antisymmetric stretching) [23]
	1640	H-O-H (deformation)
		[25–27]
	3397	O-H (valence) [25,27]
Clinochlor $(Mg,Fe)_{4.75}Al_{1.25}[Si_{2.75}Al_{1.25}O_{10}](OH)_8$ $C2/m$ [29] Three-layer grid of two silicon-oxygen tetrahedral and, aluminum oxygen separating them octahedral, layers	908	Al-OH (libration) [21–23,25]
	991	Si-O (antisymmetric stretching) [23,25,27]
	1030	
	1114, 1161	Si-O (antisymmetric stretching) [22,23, 25,26]
	1640	H-O-H (deformation) [25,27]
	3397	O-H (valence) [25,27]
Corundum Al_2O_3 $R\bar{3}c$ Simple oxide	1990, 2931, 3079, 3308	Al−O [19]

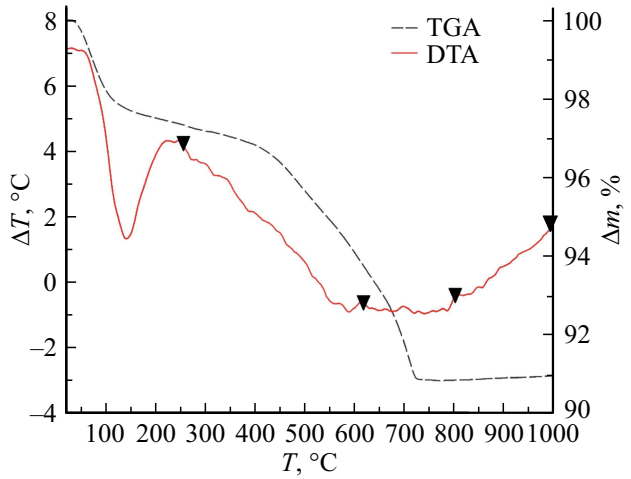

Figure 3. Differential thermal and thermogravimetric dependences for NPC.

of aluminosilicates, which may contain a weakly bound hydroxyl group (mainly clinochlorite or montmorillonite). The broad maximum at 3397 cm^{-1} also occurred due to valence fluctuations of OH groups.

Many lines of amorphous and crystalline silicon (quartz) oxides were recorded. Quartz lines are clearly visible at 693, 777 and 796 cm^{-1}. Narrow intense absorption bands of calcite are distinguishable against the background of aluminosilicates: 712, 828, 873, 1415, 1797, 2514 cm^{-1}. Their position is quite consistent with the literature [18] and allows drawing an accurate conclusion about the presence of calcite as the main carbonate. „Shoulders" are noticeable in the absorption bands. They are formed by the superposition of absorption bands of similar minerals. Most of them are shifted towards larger wavelengths relative to calcite, they are associated with distortions of crystal lattices by impurity centers because of the Jahn-Teller effect.

Low-intensity, but distinct and well consistent with the literature data, corundum absorption bands [19] are visible at the wavelengths 1990, 2931, 3079 and 3308 cm^{-1}. It can be noted that the presence of iron oxides was not found in the IR spectra, the absorption lines of which often merge with aluminosilicates [20].

Therefore, the IR spectroscopy method revealed the presence of at least 6 minerals: kaolinite, quartz, calcite, montmorillonite, clinochlore and corundum, which fully corresponds to the generally accepted definition of a polymineral complex.

2.3. Differential thermal and thermogravimetric effects in NPC samples

Fig. 3 shows a thermogram describing differential thermal and thermogravimetric effects in mineral particles. The initial samples were treated with 30% hydrogen peroxide to abandon the energy effects caused by the burning of organic matter [30]. The violent reaction with the release of hydrogen sulfide resulted in a mass loss of about 1.5 wt.

Kaolinite, montmorillonite and clinochlorite (layered silicates) are characterized by a number of endothermic effects associated with the removal of physically and chemically bound water and decomposition processes.

The first intense endothermic effect in the temperature range from 50 to 250°C (with a maximum at 140°C) is interpreted as the removal of absorbtionally bound (hydrated) and interlayer molecular water from kaolinite and montmorillonite lattices. The second endothermic effect in the temperature range from 250 to 620°C is attributable to the removal of crystallization water from these minerals and their partial amorphization [31].

Two endothermic effects on the thermogram are characteristic for the removal of crystallization and combined water from clinochlore: the first effect is in the temperature range 550−780°C, and the second is in temperature range from 750 to 950°C [32]. No similar effects were observed on the resulting thermogram, either due to the insignificant amount of clinochlore or due to the stabilization of its crystal lattice by impurity centers.

A weak endothermic effect at a temperature of about 570°C is associated with polymorphic transformations of $\alpha \rightarrow \beta$-quartz, accompanied by a slight increase of the volume of the crystal cell (by 0.82%) [28]. The exothermic process above 800°C is attributable to the started processes of particle consolidation.

The greatest mass losses are typical for the temperature ranges of 25−100°C and 450−700°C. The rate of mass loss in the first case was 0.57 g/°C, and it was 4 times greater in the second case. This is explained by various types of structural transformations such as the removal of residual organic matter and decomposition of calcite, respectively. Then the mass stabilizes up to 1000°C.

As a result, the following reference points are determined along the DTA curve, at which certain structural transformations are completed, °C: 250, 620, 800, 1000. The evolution of the NPC structure under the impact of temperature was monitored by X-ray phase analysis and ESR spectroscopy at reference points.

2.4. Evolution of the NPC phase composition under temperature impact

The isolation and analysis of clay minerals in the studied sample is possible only in case of a special sample preparation by enriching the sample with clay minerals using flotation [33]. After that, the diffractograms in the zone of small angles demonstrated a sharp increase of clay mineral intensity (Fig. 4). It was found as a result of X-ray diffraction analysis that the NPC is a polyphase system consisting of 10 phases (in descending order): α-quartz SiO_2; calcite; kaolinite; montmorillonite; microcline $K[AlSi_3O_8]$ $(P\bar{1})$, muscovite $KAl_2[AlSi_3O_{10}][OH]_2$ $(C2/c)$; clinochlore; corundum; magnetite Fe_3O_4 $(FeO{\cdot}Fe_2O_3)$ $(Fd\bar{3}m)$; rhodonite $Mn_3[Si_3O_9]$ $(P\bar{1})$.

These results are in good agreement with the data obtained by DTA/TGA, IR and XRD spectroscopy methods. Thus, the presence of microcline and muscovite is

consistent with a significant potassium content identified by XRD spectroscopy. The presence of magnetite correlates with the chemical composition, and the presence of quartz, corundum, calcite, kaolinite, montmorillonite and clinochlore correlates with IR spectroscopy data.

X-ray diffraction analysis of samples burnt at reference temperatures showed the following results (Fig. 5). The quartz content in the initial sample accounts for the half of the crystalline phases, less than in the other phases. The proportion of crystalline silicon oxides increases especially significantly after 620°C, when cristobalite (high-temperature quartz) occurs. After 1000°C, a glass phase is formed, in which part of the crystalline modifications SiO_2 is dissolved.

The calcite content decreases monotonously from 15 to 0% after heating to 800°C. This behavior of calcite is not typical, since its decomposition is expected in the temperature range from 800 to 950°C. Probably, this behavior of calcite can be explained by a strong deformation of its crystal structure by isomorphic substitutions (for example, Fe and Mn ions). The decomposition of calcite results in the formation of the X-ray amorphous oxide CaO [34]. The amorphization and decomposition of calcite turn out to be the most significant effect of reduction of the crystalline phase content.

Kaolinite and montmorillonite are contained in small amounts; their content slightly decreases after annealing at 800°C. Both phases disappear as a result of heating to 1000°C, which is also typical for these minerals [30].

Clinochlore remains stable at temperatures below 800°C and completely decomposes at 1000°C, which is typical for these minerals [35]. Microcline (potassium spar) and muscovite are thermally stable at all temperatures

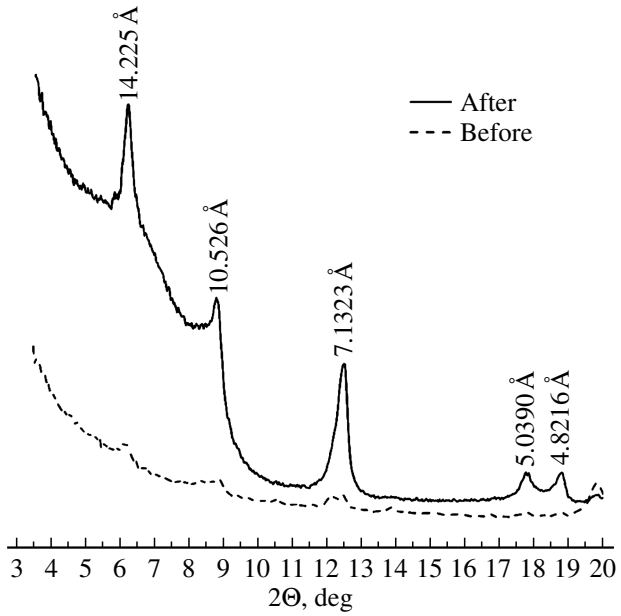

Figure 4. The intensity of the diffraction maxima in the NPC before (solid line) and after (dashed line) special sample preparation; the interplane distances are indicated.

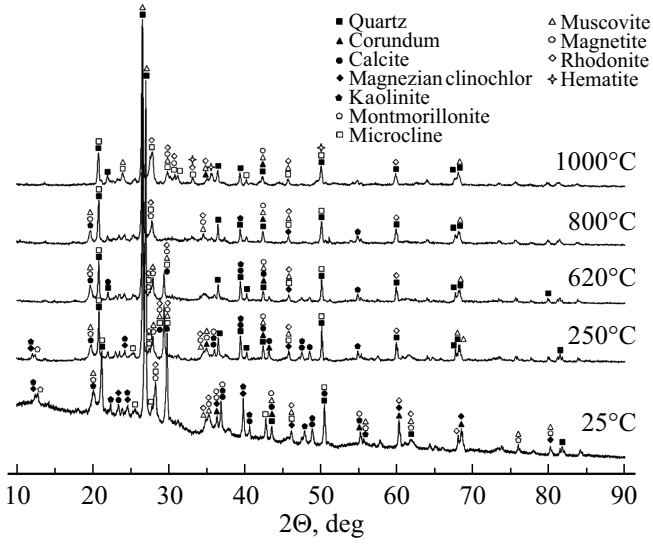

Figure 5. Diffractograms of samples burned at reference temperatures.

considered. Their relative content decreased slightly at 1000°C, since part of the phases amorphized and formed a glass phase.

The volume fraction of such phases as corundum, magnetite (hematite observed after 1000°C) and rhodonite does not change, which is typical for these crystalline structures [36–38].

As shown by quantitative X-ray phase analysis, the total volume of crystalline phases changes as a result of heat treatment, decreasing by 22% after firing at 1000°C. Silicon dioxide modifications account for about half of the crystalline phases, the relative content of which increases with temperature, reaching a maximum at 800°C. This is attributable to the occurrence of a new polymorphic modification of β-quartz. After annealing at 1000°C quartz and cristobalite, formed by the silica of the destroyed lattices of clay minerals from the crystalline phases are present in gross amounts similar to the results of [5].

2.5. Paramagnetic centers in the structure of NPC components

Obtaining of information about the fine structural and crystal chemical characteristics of minerals is an important stage of the study of natural objects. The ESR method is widely used to identify such structural features of minerals as the nature of isomorphism, defects in the crystal structure. Free radicals, molecular ions and other paramagnetic centers (PC) are suitable for the express analysis of the mineral composition of some polycrystalline and finely dispersed components of rocks [39]. The sensitivity of the ESR method, depending on the type of paramagnetic centers, reaches 0.08−0.10% in qualitative mineralogical analysis. Narrow lines of paramagnetic defects in the electronic structure such as localized unpaired electrons and holes are often observed in the ESR spectra of

aluminosilicates in addition to metal ion lines. Both types of centers such as electronic and hole centers have values of g-factors which are close to $g \approx 2.00$. Electron charged centers are believed [40,41] to be characterized by the values of $g \leq 2.00$, and the hole centers are characterized by the values of $g \geq 2.00$, therefore, it is possible to accurately determine their localization from the ESR spectra.

Fig. 6 shows the overview ESR spectra of NPC particles in the initial state and after annealing at temperatures of 250, 620, 800 and 1000°C.

The ESR spectrum of the initial sample contained one broad ($\Delta B \approx 45$ mT) low-field line with a g factor of about 4.0 and two satellite lines with $g \approx 5.327$ and ≈ 3.917. These lines are found in the ESR spectra of crystalline and amorphous substances and are usually attributed to ions Fe^{3+} in the aluminosilicate lattice. The line with $g \approx 3.7$ is associated with isomorphic processes in the pair $Fe^{3+} \rightarrow Mg^{2+}$ [42] and therefore can be attributed to clinochlore which is rich in similar isomorphic substitutions. Spectroscopy of Fe^{2+} ions in natural crystals is represented by only a small number of studies. In this case, the spin states are singlet ones that are not registered by the standard X-band equipment [43]. They are usually in tetrahedral positions, replacing silicon ions.

The lines of Cu^{2+} ions are observed in the middle magnetic fields. They are typical for axially symmetric crystal fields (tetragonal or trigonal), where the ground state is a spin doublet. Typical values: $g_{II} \approx 2.3-2.4$ and $\approx 2.0-2.2$ [40]. Moreover, both the nuclei ^{63}Si and the nuclei ^{65}Si have the spin 3/2, which results in the formation of a four-line hyperfine structure. These 4 lines were characterized by g-factors 2.4709, 2.4068, 2.3445 and 2.2319 with $A_{cu} \approx 14.65 \pm 0.1$ mT in our case. These ions were located in the interlayer space of smectites, probably montmorillonite in this case [44].

A broad intense line with $g \approx 2.10$ was identified as a ferromagnetic resonance line of magnetite particles [17]. It

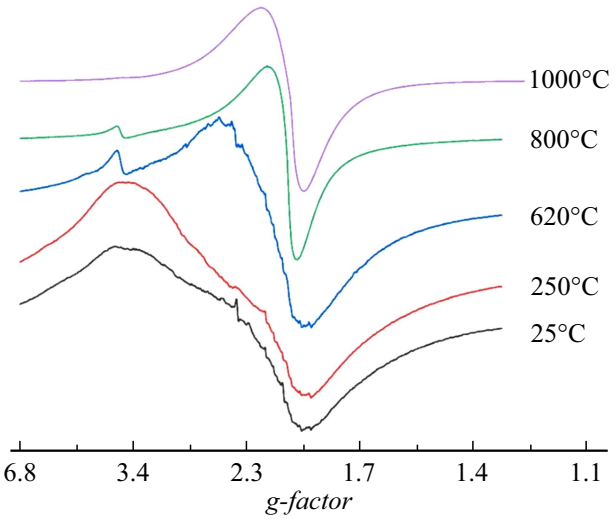

Figure 6. Transformation of the ESR spectrum of a NPC sample during high-temperature annealing.

was overlaid with sextets of an hyperfine structure caused by isomorphic ions Mn^{2+}, which substitute the main ions in both octahedral sheets of smectites and calcite. The sextet of the first type of Mn^{2+} is characterized by doublet splits caused by interactions with OH groups with g-factor equal to 1.9613 and $A_{Mn(I)} \approx 9.976$ mT. The sextet of the second type of Mn^{2+} is not burdened with duplets, for it $g \approx 1.9829$, $A_{Mn(II)} \approx 9.756$ mT. This type of Mn^{2+} is localized in calcite as a structural impurity based on the substitution scheme $Mn^{2+} \rightarrow Ca^{2+}$. The basis for this statement was the disappearance of this doublet after the decomposition of carbonates in the NPC by hydrochloric acid.

The lines with $g = 2.0016$ and 1.9789 are attributable to electron-hole centers formed during isomorphic substitutions of cations in the octahedral layer — these are the centers of O^-, which were stabilizers of $Mg^{2+} \rightarrow Al^{3+}$ substitution. They are relatively poorly related to the structure of the mineral and served as indicators of the influence of external influences on the structural ordering of the mineral.

A narrow line with $g \approx 3.578$ appeared at a low magnetic field after annealing at 620°C instead of a broad line that existed up to high temperatures and with decreasing width and amplitude, attributed to isomorphic substitution of $Fe^{3+} \rightarrow Mg^{2+}$ in clinochlore.

Calcite decomposition at 800°C resulted in the disappearance of one of the sextets Mn^{2+} with large values of g-factor and hyperfine constant $A_{Mn(II)}$. The copper lines disappeared along with the interlayer water of the smectites. This annealing temperature ensured the appearance of a narrow intense line Fe^{3+} in a strong magnetic field. The manganese sextet with $g \approx 1.9668$ and $A_{Mn(I)} \approx 8.974$ mT has been preserved along with the smectites

The annealing at a temperature of 1000°C practically did not change the position, width or shape of the magnetic resonance line Fe^{3+} with $g \approx 2.0$. The overlapping line with $g \approx 2.06$ slightly expanded. Probably, the diffusion of ions Mn^{2+} caused the formation of nonparamagnetic clusters from the ions during the decomposition of mineral lattices [45].

Therefore:

— there are two types of manganese sextets (isorphic ions in calcite and smectites) in the initial ESR spectrum, a quartet of ion lines Cu^{2+} and broad lines of Fe^{3+} with factors of about 4.0 and 2.0;

— a narrow weak line with $g \approx 3.578$ appeared after heating to 620°C, instead of a wide low-field line because of isomorphic substitution of $Fe^{3+} \rightarrow Mg^{2+}$ (probably in clinochlore). Although it decreased in width and amplitude, it was observed at a temperature of up to 1000°C;

— one of the sextets Mn^{2+} disappeared after 800°C, but a broad line with $g \approx 2.06$ appeared. Calcite decomposed, and its impurity manganese ions formed clusters;

— further heating resulted in the strengthening of broad high-field lines of manganese and iron, and the disappearance of the last sextet.

The chromium and nickel lines are indistinguishable, probably due to the low concentration of PC in the sample (less than 0.05%). Titanium lines are also indistinguishable due to the correct substitution of $Si^{4+} \rightarrow Ti^{4+}$ in the tetrahedral layer [46].

Conclusion

A set of physico-chemical analysis methods has been selected for the analysis of NPC to study the temperature evolution of the phase composition and structural transformations of the crystalline components. None of the methods is redundant in the case of the variable composition of the components and their innate tendency to isomorphic substitutions. The presence of ten crystalline phases was found by IR spectroscopy and diffractometry methods in the NPC (in descending order): α-quartz SiO_2, calcite, kaolinite, montmorillonite, microcline, muscovite, clinochlore, corundum, magnetite, rhodonite. Impurity centers were found to play an ambiguous role in the evolution of the natural mineral structures, ensuring both stabilization of their crystal lattices and distorting them due to the Jahn-Teller effect. This is most likely for layered lattices containing octahedral crystal cells with central impurity ions. The impurity centers Fe^{3+} and Mn^{2+}, which serve as labels of structural transformations, were proved to form clusters with each other as a result of the destruction of crystalline components and become „invisible“ for spectral analysis methods, but perhaps more accessible for external influences.

Conflict of interest

The authors declare that they have no conflict of interest.

References

[1] V.P. Isupov, O.A. Kharlamova, L.E. Chupakhina, M.R. Sharafutdinov, D.F. Khabibulin, O.B. Lapina. Neorgan. mater, **47** (7), 849 (2011) (in Russian).

[2] D.A. Zyuzin, E.M. Moroz, N.A. Pakhomov, G.R. Karagedov. Izvestiya RAN. Seriya fizicheskaya, **71** (5), 637 (2007) (in Russian).

[3] E.V. Edinach, Yu.A. Uspenskaya, A.S. Gurin, R.A. Babunts, G.R. Asatryan, N.G. Romanov, A.G. Badalyan, P. G. Baranov. Phys. Solid State, **61** (10), 1820 (2019). DOI: 10.1134/S1063783419100135

[4] V.A. Vazhenin, A.P. Potapov, M.Yu. Artyomov, A.V. Fokin. Phys. Solid State, **63** (5), 764 (2021). DOI: 10.1134/S106378342105019X

[5] A.A. Glebova, M.S. Skovorodnikova, I.A. Pavlova, E.P. Farafontova. Steklo i keramika, **95** (12(1140)), 27 (2022) (in Russian). DOI: 10.14489/glc.2022.12.pp.027-034

[6] A.A. Smorokov, A.S. Kantaev, D.V. Bryankin, A.A. Miklashevich. Izvestiya Tomskogo politekh. un-ta. Inzhiniring georesursov, **333** (4), 27 (2022). DOI: 10.18799/24131830/2022/4/3459

[7] A. Smorokov, A. Kantaev, D. Bryankin, A. Miklashevich, M. Kamarou, V. Romanovski. Minerals Engineering, **189**, 107909 (2022). DOI: 10.1016/j.mineng.2022.107909

[8] A. Smorokov, A. Kantaev, D. Bryankin, A. Miklashevich, M. Kamarou, V. Romanovski. J. Chem. Technol. Biotechnol., 726 (2022). DOI: 10.1002/jctb.7277

[9] A.A. Smorokov, A.S. Kantaev, D.V. Bryankin, A.A. Miklashevich. Izvestiya Vuzov. Khimiya i khimicheskaya tekhnologiya, **65** (2) 127 (2022) (in Russian). DOI: 10.6060/ivkkt.20226502.6551

[10] GOST 21216-2014. *Clay raw materials. Test methods.* (2015) (in Russian), https://docs.cntd.ru/document/1200115068

[11] O.N. Kanygina, O.P. Kushnareva, E.V. Salnikova, A.A. Yudin. Steklo i keramika, **95** (12(1140)), 41 (2022) (in Russian). DOI: 10.14489/glc.2022.12.pp.041-049

[12] O.P. Kushnareva, A.G. Chetverikova, D.K. Chetverikova. V sb: *Universitetskij kompleks kak regional'nyj centr obrazovaniya, nauki i kul'tury* (OSU, Orenburg, 2023) (in Russian).

[13] D.M. Moore, Jr. R.C. Reynolds. *X-ray Diffraction and the Identification and Analysis of Clay Minerals* (OUP, Oxford, 1989)

[14] GOST 9169-2021. *Clay raw materials for the ceramic industry. Classification* (2022) (in Russian) https://docs.cntd.ru/document/1200180651

[15] M.M. Filyak, A.G. Chetverikova, O.N. Kanygina. Kondensirovannye sredy i mezhfaznye granitsy, **20** (1), 156 (2018) (in Russian). DOI: 10.17308/kcmf.2018.20/487

[16] N.G. Reznikov, A.G. Zhikharev. Nauchnyj rezul'tat. Informatsionnyie tekhnolgii, **6** (3), 65 (2021) (in Russian). DOI: 10.18413/2518-1092-2021-6-3-0-9

[17] A.G. Chetverikova, O.N. Kanygina, V.N. Makarov, V.L. Berdinskiy, M.M. Seregin. Ceramica, **68** (388), 441 (2022). DOI: 10.1590/0366-69132022683883346

[18] G. Jovanovski, V. Stefov, B. Shoptrajanov, B. Boev. Min. Abh, **404**, 1 (2002).

[19] V. Karantoni, S. Karampelas, P. Voudouris, V. Melfos, L. Papadopoulou, T. Soldatos, C. Mavrogonatos. Minerals, **11** (7), 750 (2021). DOI: 10.3390/min11070750

[20] I.I. Plyusnina. *Infrakrasnye spektry mineralov* (Izd-vo Mosk. un-ta, M., 1976) (in Russian).

[21] A. Tironia, M.A. Trezzaa, E.F. Irassara, A.N. Scianb. Proced. Mater. Sci., **1**, 343 (2012). DOI: 10.1016/j.mspro.2012.06.046

[22] V.C. Khang, M.V. Korovkin, L.G. Ananyeva. IOP Conf. Series: Earth and Environmental Sci., **43** (1), 012004 (2016). DOI: 10.1088/1755-1315/43/1/012004

[23] J.E.F.C. Gardolinski. *Interlayer Grafting and Delamination of Kaolinite* (Kiel, 2005), 250 p.

[24] M.S.L. Rosa, R.A.O. Silva, P.E. Sousa, R.T. Nascimento, T. Knoerzer, M.R.M.C. Santos. Cerãmica, **68**, 75 (2022). DOI: 10.1590/0366-69132022683853175

[25] B. Tyagi, C.D. Chudasama, R.V. Jasra. Spectrochimica Acta Part A: Molecular and Biomolecular Spectroscopy, **64** (2), 273 (2006). DOI: 10.1016/j.saa.2005.07.018

[26] S. Tosoni, K. Doll, P. Ugliengo. Chem. Mater., **18** (8), 2135 (2006). DOI: 10.1021/cm060227e

[27] G. Jovanovski, P. Makreski. Macedonian J. Chem. Chem. Eng., **32** (2), 125 (2016). DOI: 10.20450/mjcce.2016.1047

[28] H.H. Fricke, M. Mattenklott, H. Parlar, A. Hartwig, MAK Commission. The MAK-Collection for Occupational Health and Safety: Annual Thresholds and Classifications for the Workplace, **1** (1), 401 (2002). DOI: 10.1002/3527600418.am0sio2fste2015

[29] G. Ulian, D. Moro, G. Valdrè. Appl. Clay Sci., **197**, 105779 (2020). DOI: 10.1016/j.clay.2020.105779
[30] R.E. Grim. *Applied Clay Mineralogy* (McGraw-Hill, NY., 1962)
[31] I.A. Levitsky, O.N. Khoruzhik. Steklo i keramika, **94** (5), 26 (2021) (in Russian).
[32] L.P. Ogorodova, L.V. Melchakova, M.F. Vigasina, I.A. Kiseleva, I.A. Bryzgalov. Geokhimiya, **3**, 230 (2017) (in Russian).
[33] M.V. Shaldybin, M.J. Wilson, L. Wilson, Yu.M. Lopushnyak, E.S. Kondrashova, I.V. Rychkova, M.A. Rudmin, P.B. Molokov, A.V. Muslimova. Catena, **181**, 104056 (2019). DOI: 10.1016/j.catena.2019.05.002
[34] V.F. Pavlov, A.V. Lineitsev, I.V. Pavlov, V.F. Shabanov. Glass Phys. Chem., **35** (5), 548 (2009).
[35] E. Kłosek-Wawrzyn, J. Małolepszy, P. Murzyn. Proced. Eng., **57**, 572 (2013). DOI: 10.1016/j.proeng.2013.04.073
[36] A.N. Amatuni, E.B. Shevchenko, T.I. Malyutina. TBT, **16** (3), 542 (1978) (in Russian).
[37] Y. Grosu, A. Faik, I. Ortega-Fernández, B. D'Aguanno. Solar Energy Mater. Solar Cells, **161**, 170 (2017). DOI: 10.1016/j.solmat.2016.12.006
[38] A.D. Iams, J.S. Keist, L.A. Giannuzzi, T.A. Palmer. Metallurgical and Materials Transactions A, **52** (8), 3401 (2021). DOI: 10.1007/s11661-021-06311-8
[39] V.A. Grevtsev, T.Z. Lygina. Razvedka i okhrana nedr, **8**, 34 (2010) (in Russian).
[40] P.L. Hall. Clay Minerals, **15** (4), 321 (1980). DOI: 10.1180/claymin.1980.015.4.01
[41] J. Babińska, K. Dyrek, P. Wyszomirski. Mineralogia, **38** (2), 125 (2007). DOI: 10.2478/v10002-007-0021-x
[42] S.V. Kudashev, Y.M. Shul'ga. Rus. J. Phys. Chem. A, **92** (10), 1953 (2018). DOI: 10.1134/S0036024418100151
[43] G.S. Shakurov, R.I. Khaibullin, V.G. Thomas, D.A. Fursenko, R.I. Mashkovtsev, O.N. Lopatin, A.G. Nikolaev, B.P. Gorshunov, E.S. Zhukova. FTT **59**, 8, 1576 (2017) (in Russian). DOI: 10.21883/FTT.2017.08.44761.37
[44] V.I. Osipov, V.N. Sokolov. *Gliny i ih svojstva. Sostav, stroenie i formirovanie svojstv* (Geos, M., 2013)
[45] J.R.B. Paião, S. Watanabe. Phys. Chem. Minerals, **35**, 535 (2008). DOI: 10.1007/s00269-008-0247-1
[46] A. Djemai, E. Balan, G. Morin, G. Hernandez, J.C. Labbe, J.P. Muller. J. American Ceramic Society, **84** (5), 1017 (2001). DOI: 10.1111/j.1151-2916.2001.tb00784.x

Translated by A.Akhtyamov